applied sciences

MDPI

Article

Local Non-Similar Solution for Non-Isothermal Electroconductive Radiative Stretching Boundary Layer Heat Transfer with Aligned Magnetic Field

Mohammad Ferdows [1,*], Ashish Barmon [2], Osman Anwar Bég [3], MD Shamshuddin [4] and Shuyu Sun [5]

[1] Research Group of Fluid Flow Modeling and Simulation, Department of Applied Mathematics, University of Dhaka, Dhaka 1000, Bangladesh
[2] Department of Mathematics, Khulna University of Engineering and Technology, Khulna 9203, Bangladesh
[3] Multi-Physical Engineering Sciences Group, Mechanical Engineering Department, School of Science, Engineering and Environment (SEE), University of Salford, Manchester M5 4WT, UK
[4] Department of Mathematics, School of Sciences, SR University, Warangal 506371, India
[5] Physical and Engineering Division, King Abdullah University of Science and Technology, Thuwal 23955-6900, Saudi Arabia
* Correspondence: ferdows@du.ac.bd

Abstract: Continuous two-dimensional boundary layer heat transfer in an electroconductive Newtonian fluid from a stretching surface that is biased by a magnetic field aligned with thermal radiation is the subject of this study. The effects of magnetic induction are induced because the Reynolds number is not small. The sheet is traveling with a temperature and velocity that are inversely related to how far away from the steady edge it is from the plane in which it is traveling. We also imposed external velocity $u = u_e(x) = Dx^p$ in the boundary. The necessary major equations are made dimensionless by the local non-similarity transformation and become a system of non-linear ordinary differential equations after being transformed from non-linear partial differential equations. The subsequent numerical solution of the arisen non-dimensional boundary value problem utilizes a sixth-order Runge–Kutta integration scheme and Nachtsheim–Swigert shooting iterative technique. A good correlation is seen when the solutions are compared to previously published results from the literature. Through the use of graphical representation, the physical impacts of the fluid parameters on speed, induced magnetic field, and temperature distribution are carried out. Furthermore, the distributions for skin friction coefficient and local Nusselt number are also studied for different scenarios. The skin friction coefficient and local Nusselt number are observed to increase with greater values of the temperature exponent parameter and velocity exponent parameter. However, as heat radiation increases, the local Nusselt number decreases even though temperatures are noticeably higher. The study finds applications in magnetic polymer fabrication systems.

Keywords: non-similar solution; stretching surface; induced magnetic field; velocity exponent parameter; temperature exponent parameter; boundary layers; thermal convection; radiation; electroconductive materials processing

Citation: Ferdows, M.; Barmon, A.; Bég, O.A.; Shamshuddin, M.; Sun, S. Local Non-Similar Solution for Non-Isothermal Electroconductive Radiative Stretching Boundary Layer Heat Transfer with Aligned Magnetic Field. *Appl. Sci.* **2023**, *13*, 4592. https://doi.org/10.3390/app13074592

Academic Editors: Giangiacomo Minak and Francesca Scargiali

Received: 9 January 2023
Revised: 14 March 2023
Accepted: 23 March 2023
Published: 5 April 2023

1. Introduction

Boundary-layer theory [1] remains one of the most versatile and enduring approaches in modern fluid dynamics. Introduced by the great aerospace engineer, Prandtl over a century ago, the bisection of the flow field into two distinct areas simplifies the equations of fluid flow: one in the core of the boundary layer, where the dominance of viscosity is observed and a created body which is submerged in a fluid experienced the majority of the drag force, and another side of the boundary layer where the viscosity has no significant effects on the solution and thus can be neglected. The theory has been deployed in practically every branch of fluid dynamics, including aerodynamics, medical flows, atmospheric phenomena, sediment transport, chemical engineering transport and materials processing systems, to name a few applications. In materials fabrication technologies [2], boundary layer flow with heat transfer adjacent to a stretching sheet that is moving in its own plane constitutes a fundamental problem. Stretching sheet transport phenomena arise in numerous manufacturing processes such as polymer extrusion, surface coating, plastic film packaging, enrobing, continuous casting of metals, spray deposition, etc. Magnetohydrodynamic materials processing [3] involves, among other areas, the synthesis of electrically conducting fluids and features in for example modern metallurgy, smart coating systems and metalworking processes. Complex electroconductive polymers [4] are also designed by the cooling of continuous sheets drawn through a quiescent or moving fluid and stretched during the drawing process. The composition of manufactured materials is particularly sensitive to the rate of heat transfer at the stretching surface since both heat and mass transfer as well as electromagnetic phenomena also occur in such stretching flows. Several different phenomena, such as magnetic induction in polymer alignment, variations in material composition, diamagnetic matter, texture formation in metals, and dampening of magnetic fields on conductive liquids are all observed. Phase conversion in both liquid-to-solid and solid-to-solid state transitions is also observed. Beginning with a continuous semi-infinite sheet traveling gradually through a fluid environment that was at rest, Sakiadis [5] pioneered the research of stretched boundary layer flows. Among the two common types of upwelling heat and mass transport, *forced convection* correlates with the setups where the velocity of the fluid rules over the other parameters and features often in thermal materials processing [6,7]. External forces drive the flow and buoyancy effects are vanishingly small. Examples include cooling systems in automotive engines and furnaces. Rahman et al. [8] studied energy convection in the formation of heat in a micropolar fluid along an inconsistent stretching sheet with a viscosity that is contingent on temperature and changing exterior temperature. Gupta et al. [9] presented detailed finite element computations for transverse magnetic field effects on electroconductive polymer convection flows from a stretching sheet. As noted earlier, electromagnetic induction may arise in flows where the magnetic Reynolds number is not vanishingly small. In addition to including the conventional Lorentzian magnetic drag force, *a separate equation for induced magnetic field conservation* must be included with appropriate wall and free stream boundary conditions for magnetic boundary layers. Many excellent studies of magnetic inductive boundary layers have been conducted for Newtonian viscous fluids along a semi-infinite flat plate without heat transfer by notably Greenspan and Carrier [10], Glauert [11], Gribben [12] (using matched asymptotic expansions) and Na [13]. The congruous energy relocation in the formation of heat problems has been considered by Tan and Wang [14] and Afzal [15]. More recently magnetoconvective stasis-point flow and energy transfer towards a reclined sheet with an induced magnetic field has been researched by Ali et al. [16]. Other studies featuring magnetic induction in materials processing and medical engineering include Ghosh et al. [17] (on oscillatory liquid metal boundary layers in permeable media), Ghosh et al. [18] (on network modeling of unsteady magnetic flow in a tilted rotating channel) and Ghosh et al. [19] (on asymptotic analysis of free convection Rayleigh flow). The Adomain Decomposition technique (ADM) was employed by Bég et al. [20] to compute squeezing flow characteristics in magnetic bio-lubricants. Usman et al. [21] investigated heat transmission of Williamson fluid in ciliated porous channels using MATLAB quadrature. Shamshuddin et al. [22] presented Keller box numerical solutions for gyrotactic magnetic bioconvection nanofluid. Bég et al. [23] used shooting and finite element methods to analyze the *hydromagnetic with induction effects, nano-polymers flow from a stretching surface.* All these studies highlighted the significant contribution that magnetic induction makes to transport (energy relocation such as impulse force and heat) characteristics.

In stretching sheet fluid dynamics, a variety of thermal and hydrodynamic wall conditions may be relevant in addition to various stretching sheet rates (linear, quadratic, cubic, exponential, etc.) as elaborated by Jaluria [7]. A linearly stretched sheet with a homogenous surface heat flux was used by Dutta et al. [24] for the computation of the temperature dispersion in the flow. In order to expand sheet boundary layer convection, changing surface temperature and linear surface stretching were both studied by Grubka and Bobba [25]. Karwe and Jaluria [26] employed finite difference methods to model mixed convection from a traveling sheet. Chen and Strobel's [27] research was conducted numerically on the combined forced and free convection in isothermal boundary layer flow from a horizontal sheet that was moving continuously. Ingham [28] analyzed the continuance of solutions for the free transportation boundary layer flow just about a constantly moving perpendicular surface with a temperature inversely correlated to the distance along the surface. Ali and Al-Yousef [29] have reported on laminar mixed convection adjacent to a uniformly moving vertical plate with wall mass flux effects. A hot, continuously stretched surface has been researched by Chen [30] using mixed convection cooling.

Thermal radiation also has a significant role in modern materials processing [31] and often accompanies convective and conductive heat transfer. The radiation effects on forced and free convection have both been studied extensively in recent years. Algebraic flux models are frequently employed in such studies since they circumvent the need to solve the full integro-differential equation of radiative transfer. A popular flux model is the Rosseland approximation which provides reasonable accuracy for optically dense flows. It has been utilized in many diverse studies in materials processing and chemical engineering (including coupled magnetohydrodynamic transport) in recent years and the reader is referred to [32–39].

In our study, we have out-stretched the study of Ali et al. [16] and Chen [30] by considering the velocity exponent, wall temperature exponent and thermal radiation effects. This constitutes the originality of this study. The Local Non-Similarity (LNS) approach proposed by Sparrow-Yu [40] is used. With the help of a shooting technique termed the Nachtsheim–Swigert [41] iteration methodology and a sixth order Runge–Kutta iterative process, numerical solutions of the modified nonlinear boundary layer equations are discovered. Validation with earlier studies [16,30] is included. Extensive visualization of transport characteristics (velocity, temperature, magnetic induction, local skin friction and local Nusselt number) is presented. The simulations are relevant to electroconductive materials processing [42].

Analysis of the boundary layer of Newtonian flow and heat transfer along a non-isothermal electroconductive radiative stretching surface under the influence of the aligned magnetic field effect has not yet been attempted. Therefore, utilizing the induced magnetic field effect, a study is conducted on the steady flow and heat transfer via a stretching surface. A second-order ordinary differential equation matching the heat equation, a third-order ordinary differential equation relating to the momentum equation, and a magnetic induction boundary layer equation are all generated via a similarity transformation. For different values of the dimensionless parameters of the issue under consideration, numerical computations up to the appropriate degree of precision were performed using the shooting iterative approach, which comprises the sixth-order Runge–Kutta integration scheme and the Nachtsheim–Swigert scheme for the purpose of illustrating the results graphically.

2. Mathematical Model

This study is concerned with the steady Newtonian hydromagnetic two-dimensional boundary layer convective heat intensity transport from a reclined surface affected by an aligned magnetic field along with thermal radiation. The sheet (e.g., electrically conducting polymer) is moving in a coplanar manner with a rate of change of distance and temperature inversely correlated with the distance from the leading edge, respectively. An external velocity $u = u_e(x) = Dx^p$ is imposed at the free stream. A slit is used at the origin to let the sheet squeeze through the fluid medium. Both the x-axis and the y-axis are pointed at the sheet. Two equal and opposing forces along the x-axis are applied to expand the sheet (see Figure 1). This moving sheet should move with a velocity that follows a power law form, i.e., $u_e = Cx^p$, while being affected by a surface heat flux. Further, a magnetic field in the y-direction is also produced as a result of the implications of a magnetic field of intensity H in the positive x-direction. The magnetic Reynolds number permits the generated magnetic field to be abandoned in contrast to an applied magnetic field. It is assumed that there is no applied electric field and that the Hall effect does not exist. The basic equations for two-dimensional steady incompressible laminar flow are given by Chen [30], Ghosh et al. [19], and Ali et al. [16].

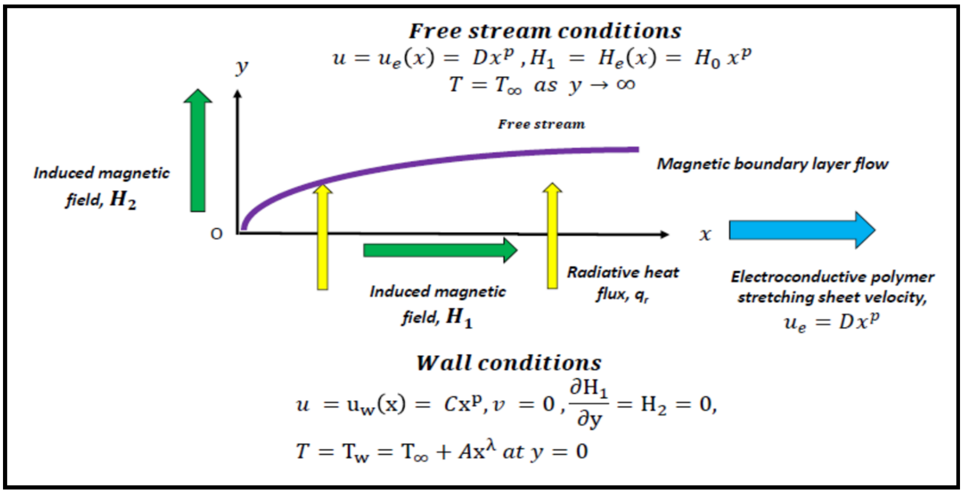

Figure 1. Magnetic boundary layer convection-radiation flow from a stretching surface.

Mass conservation (continuity)

$$\frac{\partial u}{\partial x} + \frac{\partial v}{\partial y} = 0 \tag{1}$$

Magnetic field continuity

$$\frac{\partial H_1}{\partial x} + \frac{\partial H_2}{\partial y} = 0 \tag{2}$$

Momentum

$$u\frac{\partial u}{\partial x} + v\frac{\partial u}{\partial y} - \frac{\mu}{4\pi\rho}\left(H_1\frac{\partial H_1}{\partial x} + H_2\frac{\partial H_1}{\partial y}\right) = \nu\frac{\partial^2 u}{\partial y^2} + \left(u_e\frac{du_e}{dx} - \frac{\mu H_e}{4\pi\rho}\frac{dH_e}{dx}\right) \tag{3}$$

Magnetic induction conservation

$$u\frac{\partial H_1}{\partial x} + v\frac{\partial H_1}{\partial y} - H_1\frac{\partial u}{\partial x} - H_2\frac{\partial u}{\partial y} = \mu_e\frac{\partial^2 H_1}{\partial y^2} \tag{4}$$

Energy conservation

$$u\frac{\partial T}{\partial x} + v\frac{\partial T}{\partial y} = \alpha\frac{\partial^2 T}{\partial y^2} - \frac{\partial q_r}{\partial y} \tag{5}$$

where the extended surface has cartesian coordinates x and y which are perpendicular to it, respectively. The magnetic induction units along the x and y axes are H_1 and H_2 respectively, u_e and H_e are the horizontal-velocity component and component of the horizontally produced magnetic field at the boundary layer's edge, ν is the magnetic polymer's kinematic viscosity, p is its density and μ is its dynamic viscosity, k is the fluid's thermal conductivity, c_p is its specific heat at constant pressure, and q_r is the radiative heat flux. Thermal diffusivity is symbolized as $\alpha = \frac{k}{\rho c_p}$.

Using Rosseland's estimation [32–39], the following expression of the radiative heat flux is generated

$$q_r = -\frac{4\sigma}{3k}\frac{\partial T^4}{\partial y} \tag{6}$$

where the Rosseland mean absorption coefficient is equal to k, and the Stefan–Boltzmann constant is equal to σ. According to [32–39], we disregard higher-order terms under the supposition that inside the flow, temperature variations are sufficiently modest such that Taylor series expansion can show T^4 about the free steam temperature T_∞:

$$T^4 \approx 4{T_\infty}^3\, T - 3{T_\infty}^4 \tag{7}$$

Equations (6) and (7) allow us to derive:

$$\frac{\partial q_r}{\partial y} = -\frac{16\sigma_1 {T_\infty}^3}{3k_1}\frac{\partial^2 T}{\partial y^2} \tag{8}$$

Using Equation (8) the *energy*, i.e., *thermal boundary layer* Equation (5) becomes:

$$u\frac{\partial T}{\partial x} + v\frac{\partial T}{\partial y} = \alpha\frac{\partial^2 T}{\partial y^2} - \frac{16\sigma_1 {T_\infty}^3}{3k_1}\frac{\partial^2 T}{\partial y^2} \tag{9}$$

The following are suitable border conditions:

$$\begin{cases} \mathrm{u} = \mathrm{u_w(x)} = \mathrm{Cx^p},\ \mathrm{v} = 0\,,\ \frac{\partial \mathrm{H_1}}{\partial \mathrm{y}} = \mathrm{H_2} = 0, \\ \mathrm{T} = \mathrm{T_w} = \mathrm{T_\infty} + \mathrm{Ax^\lambda} \text{ at } \mathrm{y} = 0 \\ \mathrm{u} = \mathrm{u_e(x)} = \mathrm{Dx^p}\,, \mathrm{H_1} = \mathrm{H_e(x)} = \mathrm{H_0\, x^p} \\ \mathrm{T} = \mathrm{T_\infty} \text{ as } y \to \infty \end{cases} \tag{10}$$

In this case C, D and A are constants (positive), H_0 denotes consistent magnetic field at infinity (free stream), p and λ are velocity exponent parameter and temperature exponent parameter, respectively, T_w and T_∞ are the wall temperature and the ambient temperature, respectively. The system of major equations has been transformed into a system of dimensionless equations by the introduction of the dimensionless variables listed below:

$$\begin{gathered} \eta = \tfrac{y}{x}(R_{e_x})^{\frac{1}{2}},\ \xi = \tfrac{Gr_x Cos\Upsilon}{(R_{e_x})^2},\ R_{e_x} = \tfrac{u_w}{\nu}x,\ \psi(x,y) = \nu(R_{e_x})^{\frac{1}{2}}\ f(\xi,\eta) \\ \phi = H_e\left(\tfrac{\nu x}{u_w}\right)^{\frac{1}{2}} g(\xi,\eta),\ Gr_x = \tfrac{g\beta(T_W - T_\infty)x^3}{\nu^2},\quad \theta(\xi,\eta) = \tfrac{T - T_\infty}{T_w - T_\infty} \end{gathered} \tag{11}$$

where ψ is the dimensional stream function, f is the dimensionless stream flow function, and θ is the dimensionless fluid temperature, ξ is the upthrust force variable, and η is the dimensionless interval perpendicular to the sheet. The continuity Equations (1) and (2) are now found to be identically satisfied by Equation (11). After some simplification, by substituting Equation (11) into Equations (3), (4) and (9), we obtain:

Momentum boundary layer equation

$$\begin{cases} f''' - pf'^2 + \frac{p+1}{2}ff'' + \delta^2 p + \beta\left[g'^2 p - \left(\frac{p+1}{2}\right)gg'' - p\right] = \\ (\lambda - 2p + 1)\xi\left[\frac{\partial f'}{\partial \xi}f' - \frac{\partial f}{\partial \xi}f'' + \beta\left\{g''\frac{\partial g}{\partial \xi} - g'\frac{\partial g'}{\partial \xi}\right\}\right] \end{cases} \tag{12}$$

Magnetic induction boundary layer equation

$$\gamma g''' + \frac{p+1}{2}g''f - \frac{p+1}{2}f''g = (\lambda - 2p + 1)\xi\left[\frac{\partial g'}{\partial \xi}f' - \frac{\partial f'}{\partial \xi}g' - \frac{\partial f}{\partial \xi}g'' + \frac{\partial g}{\partial \xi}f''\right] \tag{13}$$

Thermal boundary layer (heat) equation

$$\frac{1}{P_r}\left(1 + \frac{4}{3}N\right)\theta'' - \lambda f'\theta + \frac{p+1}{2}f\theta' = (\lambda - 2p + 1)\xi\left[f'\frac{\partial \theta}{\partial \xi} - \theta'\frac{\partial f}{\partial \xi}\right] \tag{14}$$

where $\beta = \frac{\mu}{4\pi\rho}\left(\frac{H_o}{C}\right)^2$ is body force magnetic parameter, a constant term $\delta = \frac{D}{C}$, $\gamma = \frac{u_e}{v}$ is the reciprocal of the magnetic Prandtl number, $P_r = \frac{\nu}{\alpha}$ is the Prandtl number and $N = \left(\frac{4\sigma T_\infty^3}{k\alpha}\right)$ is the radiation variable. The following boundary conditions are required after transformation:

$$\begin{cases} f(\xi,0) = 0,\ f'(\xi,0) = 1, \quad g(\xi,0) = 0, \\ g''(\xi,0) = 0,\ \ \theta(\xi,0) = 1 \quad\quad at\ y = 0 \\ f'(\xi,\infty) = \delta,\ \ g'(\xi,\infty) = 1,\ \ \theta(\xi,\infty) = 0\ as\ \ y \to \infty \end{cases} \tag{15}$$

Here, in this study in the computational procedure, we used the following values of parameters stated in Table 1.

Table 1. Estimated values in present study.

Parameters	Estimated Values
Magnetic parameter (β)	1, 2, 3
Upsthurst force variable (ξ)	0.5, 2.5
Velocity exponent parameter (p)	0, 0.25, 0.5, 0.55, 0.6, 0.65, 0.75, 1
Prandtl number (Pr)	0.1, 0.7, 0.72, 13
Constant parameter (δ)	3
Temperature exponent parameter (λ)	−0.75, −0.6, 0.6, −0.4, 0, 0.75, 1
Radiation parameter (N)	0, 1, 2, 3
Reciprocal of magnetic Prandtl number (γ)	0.5

Prandtl number Pr, Prandtl number with reciprocal magnetization γ, radiation variable N, magnetic force parameter β, velocity exponent parameter p, temperature exponent parameter λ, and buoyancy force parameter ξ. Results are graphically plotted in Figures 2–18.

3. Numerical Solution Using Local Non-Similarity Method (LNSM)

Numerous researchers have used the LNSM, which was proposed by Sparrow and Yu [40], for example, Minkowycz and Sparrow [43] in thermal boundary layers, Bég et al. [44] in liquid metal forced convection magnetic induction boundary layers, Hossain [45] in dissipative magnetohydrodynamic convective boundary layer flows, Bég et al. [46] in cross-diffusive magnetic boundary layers in porous media and Bég et al. [47] in inclined solar collector thermos-solutal convection boundary layers. It is an excellent technique for tackling non-similar boundary layer physics. Using this process, it is possible to extract two crucial properties from the resulting differential equations: the local solutions and the non-similar solutions at any streamwise location. The wall's unidentified boundary conditions included using a shooting approach and forward integration, two typical methods for computing the numerical solutions to these equations. The technique also permits some self-verification of the numerical results' accuracy. Considering the following transformations for the velocity, magnetic induction, and temperature fields, respectively, the LNSM retains all the terms in the altered equations with $\xi-$ derivatives:

$$\frac{\partial f}{\partial \xi} = G_1(\xi,\eta); \tag{16}$$

$$\frac{\partial g}{\partial \xi} = G_2(\xi,\eta); \tag{17}$$

$$\frac{\partial \theta}{\partial \xi} = G_3(\xi,\eta) \tag{18}$$

As a result, three new equations must be derived in order to identify $G_1(\xi,\eta)$, $G_2(\xi,\eta)$. These present three extra unknown functions. Creating the subsidiary equations by differentiating the modified equations with regard to ξ. The secondary equations for $G_1(\xi,\eta)$, $G_2(\xi,\eta)$, $G_3(\xi,\eta)$ contain the terms $\frac{\partial G_1}{\partial \xi}$, $\frac{\partial G_2}{\partial \xi}$, $\frac{\partial G_3}{\partial \xi}$ and their η derivatives. The systems of equations for $f(\xi,\eta)$, $g(\xi,\eta)$, $\theta(\xi,\eta)$, $G_1(\xi,\eta)$, $G_2(\xi,\eta)$ and $G_3(\xi,\eta)$ transmuted to an ODE (Ordinary Differential Equations) system of equations with the terms ignored. This LNS (Local Non-Similarity) technique configuration is referred to as considering that approximations are obtained by omitting the words as the second degree of truncation. The level of truncation will determine how accurate the LNS results are. Now differentiating Equations (12)–(14) with respect to ξ we have:

$$\begin{cases} \frac{\partial f'''}{\partial \xi} - 2pf'\frac{\partial f'}{\partial \xi} + \frac{p+1}{2}\left[f\frac{\partial f''}{\partial \xi} + f''\frac{\partial f}{\partial \xi}\right] + \beta\left[2g'\frac{\partial g'}{\partial \xi}p - \left(\frac{p+1}{2}\right)\left[g\frac{\partial g''}{\partial \xi} + g''\frac{\partial g}{\partial \xi}\right]\right] \\ = (\lambda - 2p + 1)\left[\frac{\partial f'}{\partial \xi}f' - \frac{\partial f}{\partial \xi}f'' + \beta\left\{\frac{\partial g}{\partial \xi}g'' - \frac{\partial g'}{\partial \xi}g'\right\}\right] + \\ (\lambda - 2p + 1)\xi\left[\left[\frac{\partial f'}{\partial \xi}\frac{\partial f'}{\partial \xi} + f'\frac{\partial^2 f''}{\partial \xi^2}\right] - \left[f''\frac{\partial^2 f}{\partial \xi^2} + \frac{\partial f}{\partial \xi}\frac{\partial f''}{\partial \xi}\right] + \right. \\ \left. \beta\left\{\left[g''\frac{\partial^2 g}{\partial \xi^2} + \frac{\partial g}{\partial \xi}\frac{\partial g''}{\partial \xi}\right] - \left[g'\frac{\partial^2 g'}{\partial \xi^2} + \frac{\partial g'}{\partial \xi}\frac{\partial g'}{\partial \xi}\right]\right\}\right] \end{cases} \tag{19}$$

$$\begin{cases} \gamma\frac{\partial g'''}{\partial \xi} + \frac{p+1}{2}\left[\frac{\partial g''}{\partial \xi}f + g''\frac{\partial f}{\partial \xi}\right] - \frac{p+1}{2}\left[f''\frac{\partial g}{\partial \xi} + g\frac{\partial f''}{\partial \xi}\right] = \\ (\lambda - 2p + 1)\left[\frac{\partial g'}{\partial \xi}f' - \frac{\partial f'}{\partial \xi}g' - \frac{\partial f}{\partial \xi}g'' + \frac{\partial g}{\partial \xi}f''\right] + (\lambda - 2p + 1)\xi\left[\left[\frac{\partial f'}{\partial \xi}\frac{\partial g'}{\partial \xi} + \frac{\partial^2 g'}{\partial \xi^2}\right]\right. \\ \left. -\left[g'\frac{\partial^2 f'}{\partial \xi^2} + \frac{\partial f'}{\partial \xi}\frac{\partial g'}{\partial \xi}\right] - \left[g''\frac{\partial^2 f}{\partial \xi^2} + \frac{\partial f}{\partial \xi}\frac{\partial g''}{\partial \xi}\right] + \left[f''\frac{\partial^2 g}{\partial \xi^2} + \frac{\partial g}{\partial \xi}\frac{\partial f''}{\partial \xi}\right]\right] \end{cases} \tag{20}$$

$$\begin{cases} \frac{1}{P_r}\left(1 + \frac{4}{3}N\right)\frac{\partial \theta''}{\partial \xi} - \lambda\left[f'\frac{\partial \theta}{\partial \xi} + \theta\frac{\partial f'}{\partial \xi}\right] + \frac{p+1}{2}\left[\theta'\frac{\partial f}{\partial \xi} + f\frac{\partial \theta'}{\partial \xi}\right] = \\ (\lambda - 2p + 1)\left[f'\frac{\partial \theta}{\partial \xi} - \theta'\frac{\partial f}{\partial \xi}\right] + (\lambda - 2p + 1)\xi\left[\left[f'\frac{\partial^2 \theta}{\partial \xi^2} + \frac{\partial \theta}{\partial \xi}\frac{\partial f'}{\partial \xi}\right] - \left[\theta'\frac{\partial^2 f}{\partial \xi^2} + \frac{\partial f}{\partial \xi}\frac{\partial \theta'}{\partial \xi}\right]\right] \end{cases} \tag{21}$$

Now applying the second level of truncation we have the following equations:

$$\begin{cases} \frac{\partial f'''}{\partial \xi} - 2pf'\frac{\partial f'}{\partial \xi} + \frac{p+1}{2}\left[f\frac{\partial f''}{\partial \xi} + f''\frac{\partial f}{\partial \xi}\right] + \beta\left[2g'\frac{\partial g'}{\partial \xi}p - \left(\frac{p+1}{2}\right)\left[g\frac{\partial g''}{\partial \xi} + g''\frac{\partial g}{\partial \xi}\right]\right] = \\ (\lambda - 2p + 1)\left[\frac{\partial f'}{\partial \xi}f' - \frac{\partial f}{\partial \xi}f'' + \beta\left\{\frac{\partial g}{\partial \xi}g'' - \frac{\partial g'}{\partial \xi}g'\right\}\right] + \\ (\lambda - 2p + 1)\xi\left[\left[\frac{\partial f'}{\partial \xi}\frac{\partial f'}{\partial \xi} + f'\frac{\partial^2 f'}{\partial \xi^2}\right] - \frac{\partial f}{\partial \xi}\frac{\partial f''}{\partial \xi} + \beta\left\{\frac{\partial g}{\partial \xi}\frac{\partial g''}{\partial \xi} - \frac{\partial g'}{\partial \xi}\frac{\partial g'}{\partial \xi}\right\}\right] \end{cases} \tag{22}$$

$$\begin{cases} \gamma\frac{\partial g'''}{\partial \xi} + \frac{p+1}{2}\left[\frac{\partial g''}{\partial \xi}f + g''\frac{\partial f}{\partial \xi}\right] - \frac{p+1}{2}\left[f''\frac{\partial g}{\partial \xi} + g\frac{\partial f''}{\partial \xi}\right] = \\ (\lambda - 2p + 1)\left[\frac{\partial g'}{\partial \xi}f' - \frac{\partial f'}{\partial \xi}g' - \frac{\partial f}{\partial \xi}g'' + \frac{\partial g}{\partial \xi}f''\right] + \\ (\lambda - 2p + 1)\xi\left[\left[\frac{\partial f'}{\partial \xi}\frac{\partial g'}{\partial \xi}\right] - \frac{\partial f'}{\partial \xi}\frac{\partial g'}{\partial \xi} - \frac{\partial f}{\partial \xi}\frac{\partial g''}{\partial \xi} + \frac{\partial g}{\partial \xi}\frac{\partial f''}{\partial \xi}\right] \end{cases} \tag{23}$$

$$\begin{cases} \frac{1}{P_r}\left(1 + \frac{4}{3}N\right)\frac{\partial \theta''}{\partial \xi} - \lambda\left[f'\frac{\partial \theta}{\partial \xi} + \theta\frac{\partial f'}{\partial \xi}\right] + \frac{p+1}{2}\left[\theta'\frac{\partial f}{\partial \xi} + f\frac{\partial \theta'}{\partial \xi}\right] = \\ (\lambda - 2p + 1)\left[f'\frac{\partial \theta}{\partial \xi} - \theta'\frac{\partial f}{\partial \xi}\right] + (\lambda - 2p + 1)\xi\left[\frac{\partial \theta}{\partial \xi}\frac{\partial f'}{\partial \xi} - \frac{\partial f}{\partial \xi}\frac{\partial \theta'}{\partial \xi}\right] \end{cases} \tag{24}$$

By introducing, $\frac{\partial f'}{\partial \xi} = G'_1(\xi,\eta)$, $\frac{\partial f''}{\partial \xi} = G''_1(\xi,\eta)$, $\frac{\partial f'''}{\partial \xi} = G'''_1(\xi,\eta)$, $\frac{\partial g'}{\partial \xi} = G'_2(\xi,\eta)$, $\frac{\partial g''}{\partial \xi} = G''_2(\xi,\eta)$, $\frac{\partial g'''}{\partial \xi} = G'''_2(\xi,\eta)$, $\frac{\partial \theta'}{\partial \xi} = G'_3(\xi,\eta)$, $\frac{\partial \theta''}{\partial \xi} = G''_3(\xi,\eta)$, the transformed equations are:

$$\begin{cases} G_1''' - 2pf'G_1' + \frac{p+1}{2}\left(G_1 f'' + fG_1''\right) + \beta\left[2g'G_2'p - \frac{p+1}{2}\left(G_2 g'' + gG_2''\right)\right] = \\ (\lambda - 2p + 1)\left[\left\{f'G_1' - f''G_1 - \beta G_2' g' + \beta G_2 g''\right\} + \xi\left\{(G_1')^2 - G_1''G_1 - \beta(G_2')^2 + \beta G_2 G_2''\right\}\right] \end{cases} \tag{25}$$

$$\begin{cases} \gamma G_2''' + \frac{p+1}{2}\left(G_1 g'' + fG_2''\right) - \frac{p+1}{2}\left(G_2 f'' + gG_1''\right) = \\ (\lambda - 2p + 1)\left[\left\{G_2'f' - G_1'g' - G_1'g'' + G_2 f''\right\} + \xi\left\{G_2 G_1'' - G_1 G_2''\right\}\right] \end{cases} \tag{26}$$

$$\begin{cases} \left(1+\frac{4}{3}N\right)G_3'' + p_r\left[\frac{p+1}{2}\left(f\,G_3' + G_1\,\theta'\right) - \lambda\left(G_3\ f' + \theta\,G_1'\right)\right] = \\ p_r(\lambda - 2p + 1)\left[\{G_3 f' - G_1\,\theta'\} + \xi\{G_3 G_1' - G_1 G_3'\}\right] \end{cases} \tag{27}$$

The border circumstances are:

$$\begin{cases} G_1(\xi,0) = 0, & G_1'(\xi,0) = 0, \\ G_1'(\xi,\infty) = 0, & G_2(\xi,0) = 0, \\ G_2'(\xi,\infty) = 0, & G_3(\xi,0) = 0, \\ G_2''(\xi,0) = 0, & G_3(\xi,\infty) = 0 \end{cases} \tag{28}$$

Finally, there are six equations that emerge and are given below:

$$\begin{cases} f''' - pf'^2 + \frac{p+1}{2} ff'' + \delta^2 p + \beta\left[g'^2 p - \left(\frac{p+1}{2}\right) gg'' - p\right] = \\ (\lambda - 2p + 1)\xi\left[\ \frac{\partial f'}{\partial \xi} f' - \frac{\partial f}{\partial \xi} f'' + \beta\{\frac{\partial g}{\partial \xi} g'' - \frac{\partial g'}{\partial \xi} g'\}\right] \end{cases} \tag{29}$$

$$\left\{\gamma g''' + \frac{p+1}{2} g'' f - \frac{p+1}{2} f'' g = (\lambda - 2p + 1)\xi\left[\frac{\partial g'}{\partial \xi} f' - \frac{\partial f'}{\partial \xi} g' - \frac{\partial f}{\partial \xi} g'' + \frac{\partial g}{\partial \xi} f''\right]\right. \tag{30}$$

$$\left\{\frac{1}{P_r}\left(1 + \frac{4}{3}N\right)\theta'' - \lambda f'\theta + \frac{p+1}{2} f\theta' = (\lambda - 2p + 1)\xi\left[f'\ \frac{\partial \theta}{\partial \xi} - \theta' \frac{\partial f}{\partial \xi}\right]\right. \tag{31}$$

$$\begin{cases} G_1''' - 2pf'G_1' + \frac{p+1}{2}\left(G_1 f'' + fG_1''\right) + \beta\left[2g'G_2'p - \frac{p+1}{2}\left(G_2 g'' + gG_2''\right)\right] = \\ (\lambda - 2p + 1)\left[\{f'G_1' - f''G_1 - \beta G_2'g' + \beta G_2 g''\} + \xi\{(G_1')^2 - G_1''G_1 - \beta(G_2')^2 + \beta G_2 G_2''\}\right] \end{cases} \tag{32}$$

$$\begin{cases} \gamma G_2''' + \frac{p+1}{2}\left(G_1 g'' + fG_2''\right) - \frac{p+1}{2}\left(G_2 f'' + gG_1''\right) = \\ (\lambda - 2p + 1)\left[\ \{G_2' f' - G_1' g' - G_1' g'' + G_2 f''\} + \xi\{G_2 G_1'' - G_1 G_2''\}\right] \end{cases} \tag{33}$$

$$\begin{cases} \left(1+\frac{4}{3}N\right)G_3'' + p_r\left[\frac{p+1}{2}\left(fG_3' + G_1\theta'\right) - \lambda\left(G_3 f' + \theta G_1'\right)\right] = \\ p_r(\lambda - 2p + 1)\left[\{G_3 f' - G_1\theta'\} + \xi\{G_3 G_1' - G_1 G_3'\}\right] \end{cases} \tag{34}$$

The combined boundary conditions are:

$$\begin{cases} f(\xi,0) = 0,\ f'(\xi,0) = 1, & G_1(\xi,0) = 0,\ G_1'(\xi,0) = 0 \\ g(\xi,0) = 0,\ g''(\xi,0) = 0 & G_1'(\xi,\infty) = 0;\ G_2(\xi,0) = 0 \\ \theta(\xi,0) = 1,\ f'(\xi,\infty)\ = \delta & G_2'(\xi,\infty) = 0;\ G_3(\xi,0) = 0 \\ g'(\xi,\infty) = 1,\ \theta(\xi,\infty) = 0 & G_2''(\xi,0) = 0,\ G_3(\xi,\infty) = 0 \end{cases} \tag{35}$$

The engineering design section has some remarkable uses of the skin friction coefficient and local Nusselt number. These parameters evaluate the wall shear stress and local wall heat transfer rate, respectively, and may be defined for the present problem as follows.

$$Skin\ Friction\ coefficient\ ,\ \ C_{fx}\left(R_{e_x}\right)^{\frac{1}{2}} = 2f''(\xi,\eta) \tag{36}$$

$$Local\ Nusselt\ number\ ,\ \ Nu_x\left(R_{e_x}\right)^{-\frac{1}{2}} = -\theta'(\xi,0) \tag{37}$$

4. Validation of Runge–Kutta Code

We have compared our results with previously well-known results and found satisfactory agreement. The comparisons are documented in Tables 2–4 and benchmarked against simpler models of Mahapattra and Gupta [48] and Ali et al. [16]. The Runge–Kutta code's correctness is attested to by the excellent confirmation that has been obtained.

Table 2. The Local Skin Friction coefficient for diverse values of δ when $\beta = 0$, $p = 1.0$, $\lambda = 0.0$, $N = 0.0$, $\gamma = 1.0$, $p_r = 0.72$, $\xi = 0$.

δ	Present	Mahapattra and Gupta [48]	Ali et al. [16]
0.1	−0.9698	−0.9694	−0.9694
0.2	−0.9187	−0.9181	−0.9181
0.5	−0.6675	−0.6673	−0.6673
2.0	2.0174	2.0175	2.0175
5.0	4.7293	4.7293	4.7293

Table 3. Skin Friction coefficient and the Local Nusselt number for diverse β when $p = 1.0$, $\lambda = N = 0.0$, $\gamma = 1.0$, and $p_r = 0.72$, $\delta = 3.0$, $\xi = 0.0$.

β	Present (Skin Friction Coefficient)	Ali et al. [16]	Present (Local Nusselt Number)	Ali et al. [16]
0.1	4.7093	4.70928	0.9794	0.97902
0.5	4.6280	4.62764	0.9766	0.97617
1.0	4.5225	4.52158	0.9729	0.97240
2.0	4.2993	4.29431	0.9648	0.96405
5.0	4.4589	3.43352	0.9300	0.92863

Table 4. The Local Nusselt number for various P_r when p = 1.0, λ = N = 0.0, $\gamma = 1.0$, $\delta = 3.0$, $\xi = 0.0$, $\beta = 1$.

P_r	Present (Local Nusselt Number)	Ali et al. [16]
0.07	0.3393	0.3381
0.5	0.8285	0.8274
2.0	1.5204	1.5214
6.8	2.5951	2.5978
10.0	3.0758	3.0790

5. Discussion of Graphical Results

The problem posed by nonlinear system of Equations (29)–(34) under boundary conditions (35) has been solved in MATLAB symbolic software using the Nachtsheim–Swigert [26] iteration technique along with a sixth-order Runge–Kutta iterative process. This technique is extremely efficient and stable and has been deployed in numerous previous investigations by the authors- see [33–36].

In order to consider the results, carry out calculations for various parameter values, for instance, Prandtl number Pr, Prandtl number with reciprocal magnetization γ, radiation variable N, magnetic force parameter β, velocity exponent parameter p, temperature exponent parameter λ, buoyancy force parameter ξ. Results are graphically plotted in Figures 2–18.

In Figures 2–4, it is shown how a magnetic parameter affects the induced magnetic fields' speed, temperature, and direction. It is evident that the velocity profile decreases with escalating magnetic force parameter β and increases with the increasing buoyancy force parameter ξ as shown in Figure 2. The momentum boundary layer thickness is, therefore, increased with greater magnetic Lorentz retarding force (flow retardation) whereas it is reduced with the thermal buoyancy effect. By increasing the magnetic force parameter β the temperature profile increases whereas it is reduced by increasing the upthrust force parameter ξ as shown in Figure 3. The additional energy that the magnetic polymer expends to drag against the imposed magnetic field is undoubtedly lost as thermal energy. This warms the environment and thickens the thermal-boundary layer. Increasing thermal buoyancy, however, only assists momentum development and counteracts thermal diffusion in the regime by suppressing convection currents and reducing thermal boundary layer thickness. It is also seen that the induced magnetic field profile decreases with increasing magnetic force parameter β whereas it increases with increasing buoyancy force parameter ξ as shown in Figure 4. Magnetic induction is, therefore, inhibited with Lorentz body force whereas it is encouraged with thermal buoyancy effect; this manifests in a respective thinning and thickening of magnetic boundary layer thickness, as well as numerous additional investigations, including those by Glauert [11] and Gribbin [12] among others. It is also important to note that Figure 4 specifies 0.5 for the magnetic Prandtl number's inverse $= \frac{u_e}{v}$. Physically as elaborated by Cramer and Pai [49]. When this parameter is unity the momentum and magnetic boundary layer thicknesses are approximately equal. Magnetic diffusion rate, however, outpaces momentum diffusion rate for $\gamma = 0.5$. This encourages the influence of Lorentzian body force which counteracts magnetic induction and decreases the magnetic boundary layer thickness. Asymptotically smooth distributions are computed in the free stream indicating that a sufficiently large infinity boundary condition is prescribed in the MATLAB Runge–Kutta code.

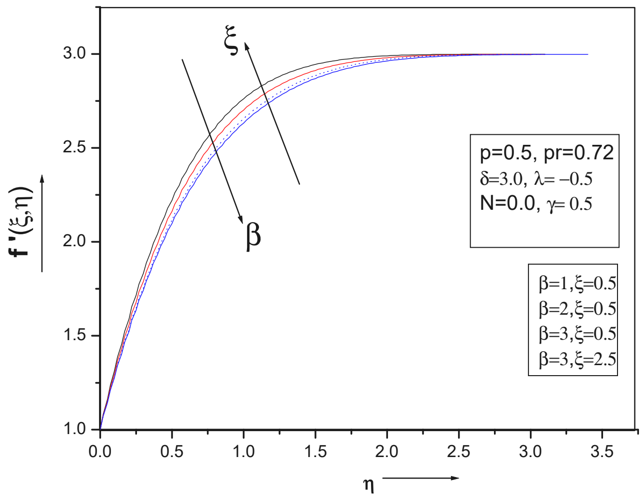

Figure 2. Effect of the body force magnetic parameter on velocity profile.

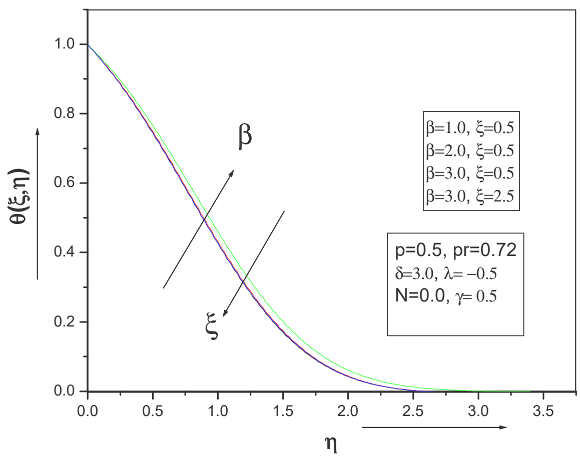

Figure 3. Effect of the magnetic force parameter on temperature profile.

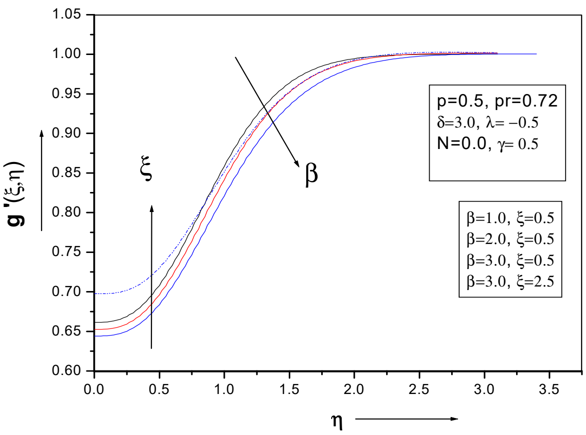

Figure 4. Effect of the magnetic force parameter on magnetic field profile.

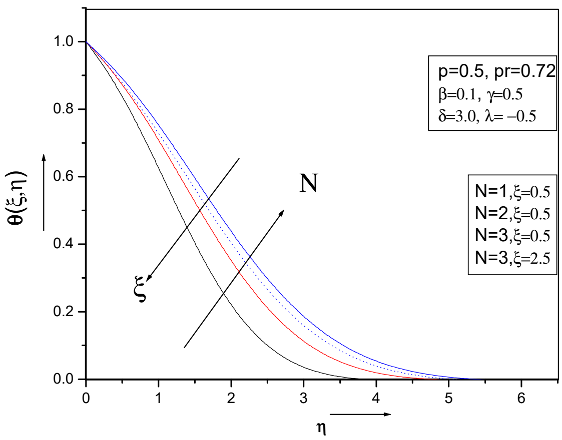

Figure 5. Effect of the radiation parameter on temperature profile.

Figure 5 shows the influence of the radiation parameter N as well as the upthrust force variable ξ on the temperature profile. The temperature profile escalates with increasing radiation variable N and declines with increasing upthrust force variable ξ. Radiation parameter N has no effect on velocity and induced magnetic field profiles, respectively, which is understandable since it does not feature in either the hydrodynamic (momentum) or magnetic induction boundary layer equations. Radiation's main impact is to energize the regime of the boundary layer, which raises temperatures and increases the thickness of the fluid energy border layer. Again, in the free stream, smooth decays are generated to demonstrate that the simulations are accurately run in MATLAB by employing an appropriately big infinity boundary condition.

The effect of temperature exponent parameter λ on the velocity, temperature and induced magnetic field profiles are given in Figures 6–8. Figure 6 shows that the speed profile deteriorates weakly with increasing temperature exponent parameter λ and increases weakly with increasing buoyancy-force parameter ξ. By rising the temperature-exponent term λ and buoyancy-force term ξ, respectively, the heat profiles are seen in Figure 7 to be strongly decreasing. The non-isothermal effect, therefore, produces lower temperature magnitudes than would be computed with an isothermal model. Again, we noticed in Figure 8 that with the rising of magnetic intensity, the contour of the induced decelerates with the acceleration of the temperature exponent parameter λ and increases with the escalating buoyancy force parameter ξ. However, the impact again is marginal, and a much more pronounced effect is observed, as expected, on the temperature distribution (Figure 7).

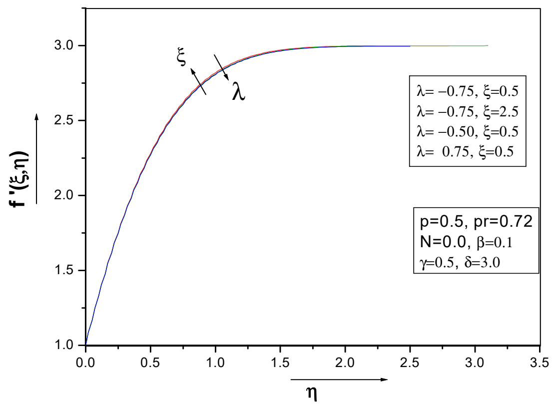

Figure 6. Effect of the temperature exponent parameter on velocity profile.

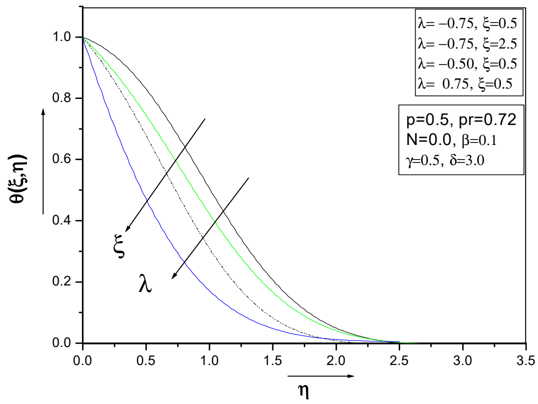

Figure 7. Effect of the temperature exponent parameter on temperature profile.

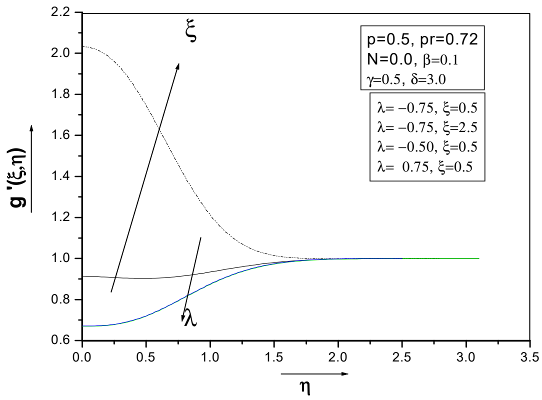

Figure 8. Effect of the temperature exponent parameter on magnetic field profile.

Velocity exponent parameter p impact on the velocity, temperature, and induced magnetic field profiles is discussed in Figures 9–11. It is seen that the velocity profile increases by increasing the value of the p ande ξ as shown in Figure 9. Substantial flow acceleration is, therefore, induced with power-law stretching and thermal buoyancy effect, i.e., the thickness of the momentum boundary layer is lowered. According to Figure 10, the thickness of the thermal boundary layer is decreased in the regime as the velocity exponent variable p, and the upthrust force variable ξ is increased. We observe from Figure 11 that the induced magnetic field profile, however, is enhanced with elevation in the value of p and ξ. Magnetic boundary layer thickness is, therefore, accentuated with power-law stretching of the sheet and stronger thermal buoyancy effect.

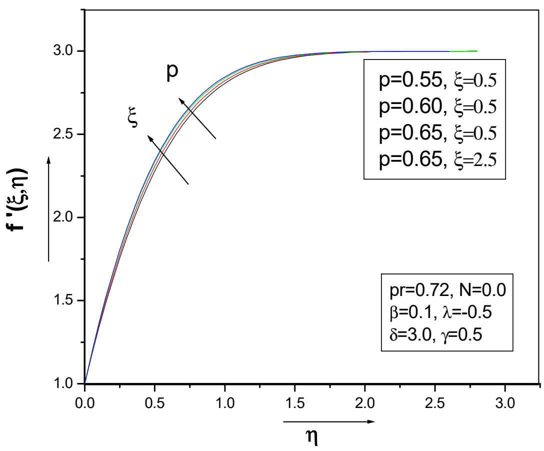

Figure 9. Effect of the velocity exponent parameter on velocity profile.

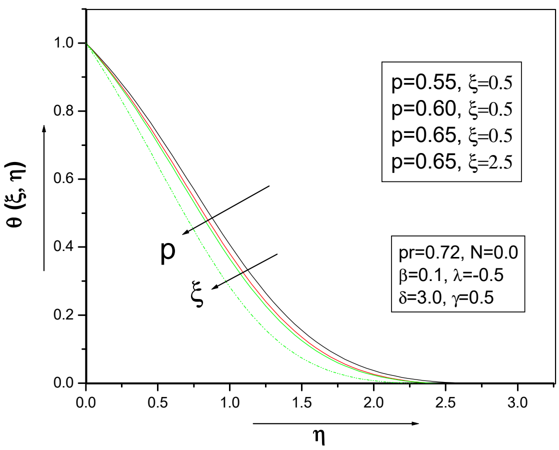

Figure 10. Effect of the velocity exponent parameter on temperature profile.

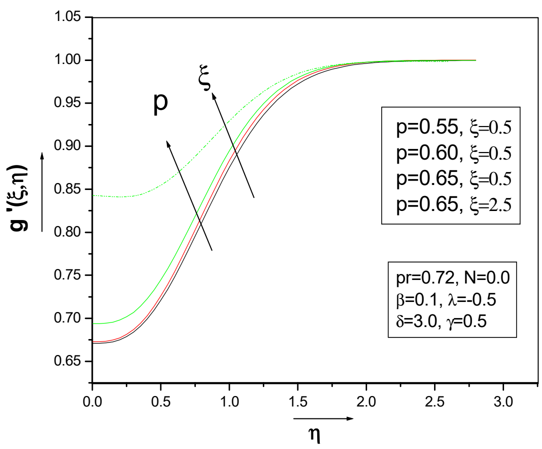

Figure 11. Effect of the velocity exponent parameter on magnetic field profile.

Figure 12 shows the effect of Prandtl number Pr on the temperature profile only. It is seen that the temperature profile declines with escalating Pr and ξ. The thickness of the energy boundary layer deteriorated with the enhancement of Pr values. The single-most prime statistic in heat transmission in fluids is the Prandtl number Pr, which is a property of a specific fluid under specific circumstances. It is inversely proportional to the fluid's thermal conductivity because it measures the relationship between momentum and thermal diffusivity. Higher thermal conductivity fluids are correlated with Lower Prandtl values and vice versa. When $Pr = 1$, the momentum and thermal diffusion rates are equal, and the thickness of the thermal and velocity boundary layers will be the same. Heat diffusion greatly surpasses momentum diffusivity when Pr is significantly low. Thermal buoyancy encourages momentum diffusion, as noted earlier, but suppresses thermal diffusion. A higher buoyancy force parameter, ξ, therefore, decreases the thickness of the thermal boundary layer.

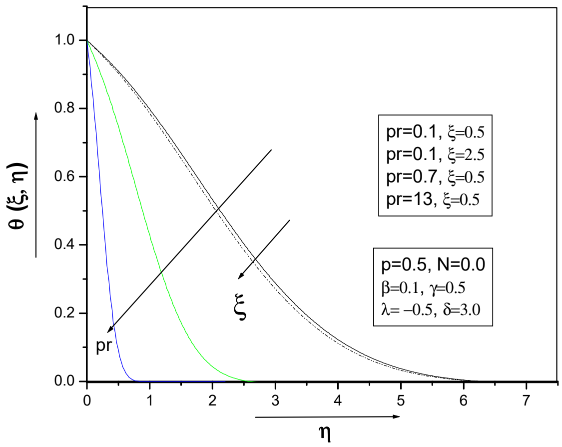

Figure 12. Effect of the Prandtl number on temperature profile.

Figures 13 and 14 display the effects of the velocity exponent parameter p on the local Nusseltl number and the local skin friction coefficient. At different values of p, Local Skin friction and Local Nusselt number are expressed as a function of ξ. The local Nusselt number grows when the buoyancy force parameter ξ and the velocity exponent parameter p increase, as seen in Figure 13. The local skin friction coefficient rises when the buoyancy force parameter and the velocity exponent parameter p, rise, as can be shown once more in Figure 14. As a result, a clearly discernible flow acceleration is produced with increased thermal buoyancy ξ,and power-law stretching velocity effects.

As illustrated in Figures 15 and 16, the "Local Nusselt number and the Local Skin Friction coefficient" are presented as a function of ξ various values of the temperature exponent parameter, λ. According to Figure 15, the local Nusselt number rises when the buoyant force parameter ξ rises for a given λ, which boosts heat transmission to the wall. As seen in Figure 16, the local skin friction coefficient increases for a given λ as the buoyancy force parameter ξ grows.

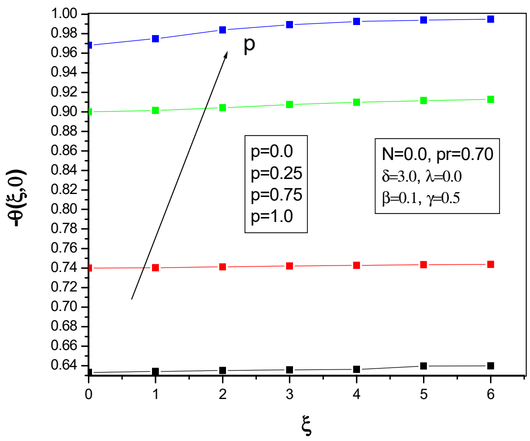

Figure 13. Effect of the velocity exponent and buoyancy force parameter on the Nusselt number.

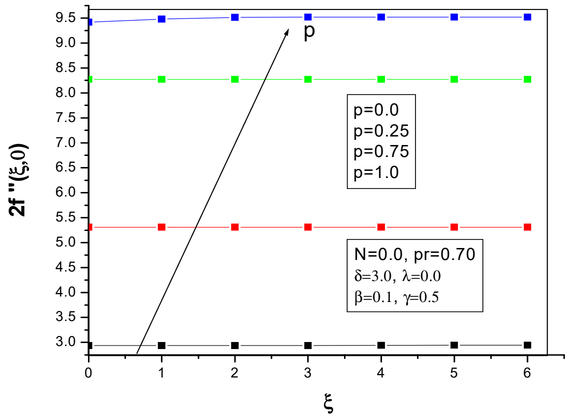

Figure 14. Effect of the velocity exponent and buoyancy force parameter on the skin friction coefficient.

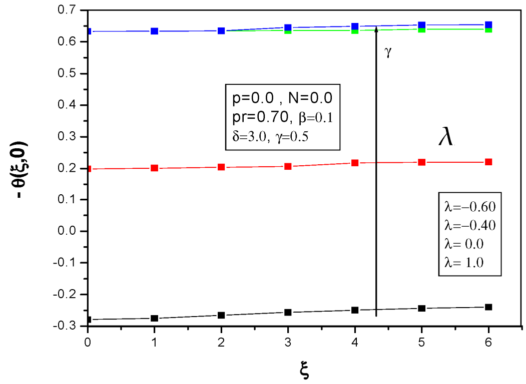

Figure 15. Effect of the temperature exponent and buoyancy force parameter on Nusselt number.

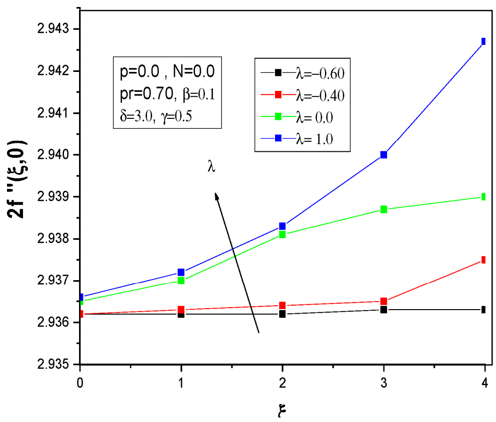

Figure 16. Effect of the temperature exponent and buoyancy force parameter on the skin friction coefficient.

The local Nusselt number and the local skin friction coefficient are presented as a function of ξ at various values of the magnetohydrodynamic force parameter, β in Figures 17 and 18. Noticed from Figure 17 that the Nusselt number increases significantly in magnitude when ξ rises for a given β. Figure 18 demonstrates that for a particular, the local drag coefficient accentuates gradually as buoyancy-force parameter ξ rises.

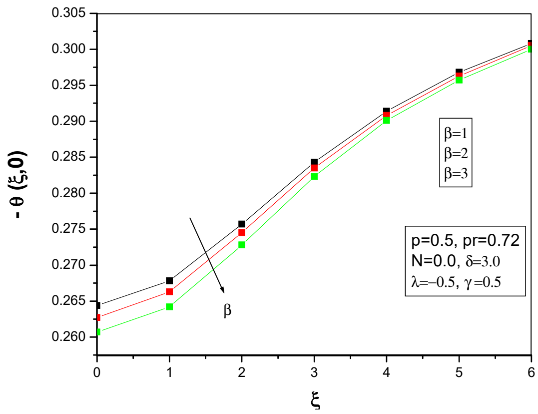

Figure 17. Effect of the magnetic field and buoyancy force parameter on the Nusselt number.

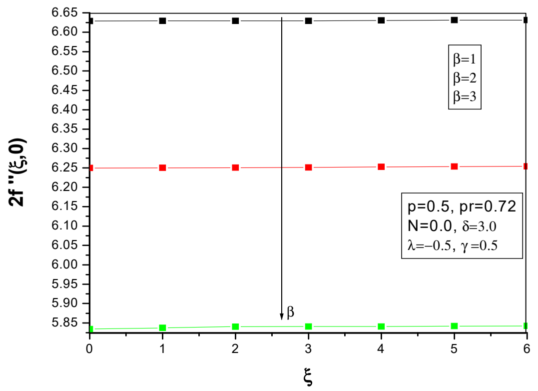

Figure 18. Effect of the magnetic field and buoyancy force parameter on the skin friction.

6. Conclusions

The processing of magnetic polymer materials at high temperatures, under the influence of an aligned magnetic field and heat radiation, has been modeled using an extensive mathematical model for steady two-dimensional boundary layer heat transmission in an electroconductive Newtonian fluid from an expanded surface. Sparrow–Yu local non-similarity transformations were used to non-dimensionalize the governing boundary layer equations, which could be solved numerically by a sixth-order Runge–Kutta integration scheme with a Nachtsheim–Swigert shooting iterative technique. The accuracy of the numerical scheme has been verified through comparison with published literature shown in Tables 2–4. The following conclusions can be drawn:

- For a given value of the buoyancy force parameter, the local Nusselt number is increased by improving the velocity exponent parameter and temperature exponent parameter and decreases by improving the magnetic force parameter, radiation parameter, and reciprocal of magnetic Prandtl number.
- For a given value of the buoyancy force parameter, the wall shear stress (local skin friction coefficient) increases with an increase in the temperature exponent parameter, reciprocal of the magnetic Prandtl number, and velocity exponent parameter, whereas it decreases with an increase in the magnetic force parameter.
- Yet, raising the buoyancy force parameter causes the temperature to decrease while increasing the velocity and magnetic induction profiles. Increasing the temperature-exponent parameter decreases the rate of change in distance, the induced magnetic field, and the temperature magnitudes.
- By increasing the magnetic force variable, the temperature is elevated but the velocity outline and magnetic field created are suppressed.

- ❖ As the radiation parameter increases, the temperature outline grows while the local Nusselt number decreases.

Some intriguing new information on the processing of thermal magnetic polymer sheets has emerged from the current simulations. They have, however, been limited to Newtonian flow. Future studies may take into account non-Newtonian models for various electroconductive polymers, such as viscoelastic [50] and viscoplastic models [51], which are now being taken into consideration.

Author Contributions: M.F. and A.B. carried out the formal analysis, investigation, conceptualization and drafted the manuscript. O.A.B. and S.S. carried out analysis, review and editing. M.S. carried out methodology, review and editing. All authors have read and agreed to the published version of the manuscript.

Funding: The authors declare that no funding was received.

Institutional Review Board Statement: Not applicable.

Informed Consent Statement: Not applicable.

Data Availability Statement: Data sharing not applicable to this article as no datasets were generated or analyzed during the current study.

Acknowledgments: We would greatly please to reviewer for their comments to improve the manuscripts.

Conflicts of Interest: The authors declare no conflict of interest.

References

1. Schlichting, H. *Boundary-Layer Theory*, 7th ed.; Mac-Graw-Hill: New York, NY, USA, 2014.
2. Zhang, S.; Zhao, D. *Advances in Magnetic Materials Processing, Properties, and Performance*; CRC Press: Boca Raton, FL, USA, 2017.
3. Schneider-Muntau, H.J.; Wada, H. Materials processing in magnetic fields. In Proceedings of the International Workshop on Materials Analysis and Processing in Magnetic Fields, Tallahassee, FL, USA, 17–19 March 2004.
4. Kuhn, H.H. *Intrinsically Conducting Polymers: An Emerging technology*; Kluwer Academic: Dodrecht, The Netherlands, 1993.
5. Sakiadis, B.C. Boundary-layer behavior on continuous solid surfaces: I. Boundary-layer equations for two-dimensional and axisymmetric flow. *AIChemE J.* **1960**, *7*, 26–28. [CrossRef]
6. Poirier, D.R.; Geiger, G.H. *Transport Phenomena in Materials Processing*; Wiley: New York, NY, USA, 1998.
7. Jaluria, Y. Thermal processing of materials: From basic research to engineering. *ASME J. Heat Trans.* **2003**, *125*, 957–979. [CrossRef]
8. Rahman, M.M.; Rahman, M.A.; Samad, M.A.; Alam, M.S. Heat transfer in a micro polar fluid along a non-linear stretching sheet with a temperature–dependent viscosity and variable surface temperature. *Int. J. Thermophys.* **2009**, *30*, 1637–1648. [CrossRef]
9. Gupta, D.; Kumar, L.; Bég, O.A.; Singh, B. Finite element simulation of nonlinear magneto-micropolar stagnation point flow from a porous stretching sheet with prescribed skin friction. *Comput. Therm. Sci.* **2015**, *7*, 1–14. [CrossRef]
10. Greenspan, H.P.; Carrier, G.F. Magnetohydrodynamic flow past a flat plate. *J. Fluid Mech.* **1959**, *6*, 77–96. [CrossRef]
11. Glauert, M.B. A study of the *magnetohydrodynamic boundary* layer on a flat plate. *J. Fluid Mech.* **1961**, *10*, 276–288. [CrossRef]
12. Gribben, R.J. The magnetohydrodynamic boundary layer in the presence of pressure gradient. *Proc. R. Soc. A* **1965**, *287*, 123–141.
13. Na, T.Y. Initial-value method for the solution of MHD boundary-layer equations. *Aeronaut. Quart.* **1970**, *21*, 91–99. [CrossRef]
14. Tan, C.W.; Wang, C.T. Heat transfer in aligned field magnetohydrodynamic flow past a flat plate. *Int. J. Heat Mass Transf.* **1968**, *11*, 319–329. [CrossRef]
15. Afzal, N. Heat transfer in MHD flow with aligned field on a flat plate at high Prandtl number. *Int. J. Heat Mass Transf.* **1972**, *15*, 863–865. [CrossRef]
16. Ali, F.M.; Nazar, R.; Arifin, N.M.; Pop, I. MHD stagnation-point flow and heat transfer towards stretching sheet with induced magnetic field. *Appl. Math. Mech. Engl. Ed.* **2011**, *32*, 409–418. [CrossRef]
17. Ghosh, S.K.; Anwar Bég, O.; Rawat, S.; Tasveer, A. Mathematical modelling of oscillatory electrically conducting liquid metal flow and heat transfer in high-porosity media with magnetic induction effects. *Int. J. Appl. Math. Mech.* **2010**, *6*, 19–38.
18. Ghosh, S.K.; Bég, O.A.; Zueco, J.; Prasad, V.R. Transient hydromagnetic flow in a rotating channel permeated by an inclined magnetic field with magnetic induction and Maxwell displacement current effects. *ZAMP J. Appl. Math. Phys.* **2010**, *61*, 147–169. [CrossRef]
19. Ghosh, S.K.; Bég, O.A.; Zueco, J. Hydromagnetic free convection Rayleigh flow with induced magnetic field effects. *Meccanica* **2010**, *45*, 175–185. [CrossRef]
20. Bég, O.A.; Tripathi, D.; Sochi, T.; Gupta, P.K. Adomian decomposition method (ADM) simulation of magneto-biotribological squeeze film with magnetic induction effects. *J. Mech. Med. Biol.* **2015**, *15*, 1550072.1–1550072.23. [CrossRef]

21. Shaheen, S.; Arain, M.B.; Nisar, K.S.; Albakri, A.; Shamshuddin, M.D.; Mallawi, F.O. A case study of heat transmission in a Williamson fluid through a ciliated porous channel: A semi-numerical approach. *Case Stud. Therm. Eng.* **2023**, *41*, 102523. [CrossRef]
22. Shamshuddin, M.D.; Rajput, G.R.; Jamshed, W.; Shahzad, F.; Salawu, S.O.; Abderrahmane, A.; Patil, V.S. MHD bioconvection microorganism nanofluid driven by a stretchable plate through porous media with an induced heat source. *Waves Random Complex Media* **2022**, 1–25. [CrossRef]
23. Anwar Bég, O.; Kuharat, S.; Ferdows, M.; Das, M.; Kadir, A.; Shamshuddin, M.D. Magnetic nano-polymer flow with magnetic induction and nanoparticle solid volume fraction effects: Solar magnetic nano-polymer fabrication simulation. *Proc. IMechE-Part N J Nanoeng. Nanomater. Nano-Syst.* **2019**, 1–19. [CrossRef]
24. Dutta, B.K.; Roy, P.; Gupta, A.S. Temperature field in flow over a stretching sheet with uniform heat flux. *Int. Comm. Heat Mass Transf.* **1985**, *12*, 89–94. [CrossRef]
25. Grubka, L.G.; Bobba, K.M. Heat transfer characteristic of a continuous stretching surface with variable temperature. *ASME J Heat Transf.* **1985**, *107*, 248–250. [CrossRef]
26. Karwe, M.V.; Jaluria, Y. Fluid flow and mixed convection transport from a moving plate in rolling and extrusion processes. *ASME J Heat Transf.* **1988**, *110*, 655–661. [CrossRef]
27. Chen, T.S.; Strobel, F.A. Buoyancy effects on boundary layer inclined, continuous, moving horizontal flat plate. *ASME J Heat Transf.* **1980**, *102*, 170–172. [CrossRef]
28. Ingham, D.B. Singular and non-unique solutions of the boundary layer equations for the flow due to free convection near a continuously moving vertical plate. *J Appl. Math. Phys. (ZAMP)* **1986**, *37*, 559–572. [CrossRef]
29. Ali, M.; Al-Yousef, F. Laminar mixed convection from a continuously moving vertical surface with suction or injection. *Int. J. Heat Mass Transf.* **1998**, *33*, 301–306. [CrossRef]
30. Chen, C.H. Mixed convection cooling of a heated, continuously stretching surface. *Int. J. Heat Mass Transf.* **2000**, *36*, 79–86. [CrossRef]
31. Mansour, R.B.; Viskanta, R. Radiative and convective heat transfer for materials processing. In *First Conference on Transport Phenomena in Processing*; Guceri, S.I., Ed.; Technomic Publishing Co.: Lancaster, PA, USA, 1992; pp. 693–713.
32. Bég, O.A.; Ghosh, S.K. Analytical study of magnetohydrodynamic radiation-convection with surface temperature oscillation/secondary flow effects. *Int. J. Appl. Math. Mech.* **2010**, *6*, 1–22.
33. Shamshuddin, M.D.; Mabood, F.; Khan, W.A.; Rajput, G.R. Exploration of thermal Peclet number, vortex viscosity and Reynolds number on two-dimensional flow of micropolar fluid through a channel due to mixed convection. *Heat Transf.* **2023**, *52*, 854–873. [CrossRef]
34. Gupta, D.; Kumar, L.; Bég, O.A.; Singh, B. Finite element simulation of mixed convection flow of micropolar fluid over a shrinking sheet with thermal radiation. *Proc IMechE- Part E J. Process Mech. Eng.* **2014**, *228*, 61–72. [CrossRef]
35. Uddin, M.J.; Bég, O.A.; Ghose, P.K.; Ismael, A.I.M. Numerical study of non-Newtonian nanofluid transport in a porous medium with multiple convective boundary conditions and nonlinear thermal radiation effects. *Int. J. Num. Meth. Heat Fluid Flow* **2016**, *26*, 1–25. [CrossRef]
36. Jamshed, W.; Eid, M.R.; Shahzad, F.; Safdar, R.; Shamshuddin, M.D. Keller box analysis for thermal efficiency of magneto time-dependent nanofluid flowing in solar-powered tractor application applying nano-metal shaped factor. *Waves Random Complex Media* **2022**, 1–36. [CrossRef]
37. Uddin, M.J.; Bég, O.A.; Uddin, M.N. Energy conversion under conjugate conduction, magneto-convection, diffusion and nonlinear radiation over a non-linearly stretching sheet with slip and multiple convective boundary conditions. *Energy* **2016**, *115*, 1119–1129. [CrossRef]
38. Shamshuddin, M.D.; Shahzad, F.; Jamshed, W.; Bég, O.A.; Eid, M.R.; Bég, T.A. Thermo-solutal stratification and chemical reaction effects on radiaitve magnetized nanofluid flow along an exponentially stretching sensor plate: Computational analysis. *J. Magn. Magn. Mat* **2023**, *565*, 170286. [CrossRef]
39. Venkatadri, K.; Bég, O.A.; Prasad, V.R. Numerical simulation of thermal radiation influence on natural convection in a trapezoidal enclosure: Heat flow visualization through energy flux vectors. *Int. J. Mech. Sci.* **2019**, *171*, 105391. [CrossRef]
40. Sparrow, E.M.; Yu, H.S. Local non-similarity thermal boundary layer solutions. *ASME J. Heat Transf.* **1971**, *93*, 328–334. [CrossRef]
41. Nachtsheim, P.R.; Swigert, P. Satisfaction of Asymptotic Boundary Conditions in Numerical Solution of Systems of Nonlinear Equations of Boundary-Layer Type. U.S. Patent NASA TN D-3004, 1 October 1965.
42. Herbert, N. Polymers, electrically conducting. In *Ullmann's Encyclopedia of Industrial Chemistry*; Wiley-VCH: New York, NY, USA, 2002.
43. Minkowycz, W.J.; Sparrow, E.M. Numerical solution scheme for local non-similarity boundary layer analysis. *Numer. Heat Transf.* **1978**, *1*, 69–85. [CrossRef]
44. Bég, O.A.; Bakier, A.Y.; Prasad, V.R.; Ghosh, S.K. Non-similar, laminar, steady, electrically conducting forced convection liquid metal boundary layer flow with induced magnetic field effects. *Int. J. Thermal. Sci.* **2009**, *48*, 1596–1606. [CrossRef]
45. Hossain, M.A. Viscous and Joule heating effects on MHD-free convection flow with variable plate temperature. *Int. J. Heat Mass. Transf.* **1992**, *35*, 3485–3487. [CrossRef]
46. Bég, O.A.; Bakier, A.Y.; Prasad, V.R. Numerical study of free convection magnetohydrodynamic heat and mass transfer from a stretching surface to a saturated porous medium with Soret and Dufour effects. *Comput. Mater. Sci.* **2009**, *46*, 57–65. [CrossRef]

47. Bég, O.A.; Bakier, A.; Prasad, V.R.; Ghosh, S.K. Numerical modelling of non-similar mixed convection heat and species transfer along an inclined solar energy collector surface with cross diffusion effects. *World J. Mech.* **2011**, *1*, 185–196. [CrossRef]
48. Mahapatra, T.R.; Gupta, A.S. Stagnation point-flow of a viscoelastic fluid towards a stretching surface. *Int. J. Non-Linear Mech.* **2004**, *39*, 811–820. [CrossRef]
49. Cramer, K.C.; Pai, S.I. *Magnetofluid Dynamics for Engineers and Applied Physicists*; McGraw-Hill: New York, NY, USA, 1973.
50. Datti, P.S.; Prasad, K.V.; Abel, M.S.; Joshi, A. MHD viscoelastic fluid flow over a non-isothermal stretching sheet. *Int. J Eng. Sci.* **2004**, *42*, 935–946. [CrossRef]
51. Bhatti, M.M.; Ullah Khan, S.; Anwar Bég, O.; Kadir, A. Differential transform solution for Hall and Ion slip effects on radiative-convective viscoplastic Casson flow from a stretching sheet with convective heating. *Heat Transf.* **2019**, *49*, 872–888. [CrossRef]